crystals

MDPI

Article

Bisphthalonitrile with a Disulfide-Based Linker and its Dimethylene Analogue: Comparative Structural Insights

Serkan Alpugan, Gülçin Ekineker, Vefa Ahsen, Savaş Berber, Emel Önal * and Fabienne Dumoulin *

Department of Chemistry, Gebze Technical University, Gebze 41400, Kocaeli, Turkey; knightofthorns@gmail.com (S.A.); generimogulcin@hotmail.com (G.E.); ahsen@gtu.edu.tr (V.A.); savasberber@gtu.edu.tr (S.B.)

* Correspondence: eonal@gtu.edu.tr (E.Ö.); fdumoulin@gtu.edu.tr (F.D.); Tel.: +90-262-605-3022 (F.D.)

Academic Editor: Helmut Cölfen

Received: 30 May 2016; Accepted: 29 July 2016; Published: 9 August 2016

Abstract: Phthalonitriles are key precursors of phthalocyanines. Self-quenching dimeric phthalocyanines likely to be cleaved into monomeric species are of potential interest for tumour-site activated photosensitisers. Disulfide linkers can be specifically cleaved in tumoral tissue do to their reductive nature. Hence, a disulfide-linked phthalonitrile was designed to serve as further precursor of specifically tumour-activatable phthalocyanine-based photosensitising systems. Bisphthalonitrile with a disulfide-based linker and its dimethylene analogue were comparatively analyzed on a spectroscopic point of view as well as with DFT calculations. A thorough crystallographic analysis of the disulfide-linked derivative was conducted.

Keywords: bisphthalonitrile; disulfide; comparative characterization; single-crystal; DFT calculations; structure optimization

1. Introduction

Photodynamic therapy is a treatment modality based on the local generation of singlet oxygen upon irradiation of a photosensitiser at appropriate wavelengths [1]. It is widely used in dermatology [2], against age-related macular degeneration [3] or for antibacterial prescription [4]. Photodynamic therapy is successfully used as well against several cancers [5], and this application gathers many efforts towards more specific and efficient photosensitising systems. Thanks to the short lifetimes of singlet oxygen, the toxicity is locally limited to the irradiation zone, which avoids the drawbacks of other therapies. Two strategies are developed to limit the photodynamic action to the tumour area, in order to preserve healthy tissues surrounding the tumour from the photodynamic effect. The first strategy is to promote the selective accumulation of the photosensitiser into tumorous tissues by conjugating it to tumour-targeting moieties [6], or the administration of photosensitiser under a photo-inactive form going to be activated only in the specific tumour conditions. In this later case, the activation should be induced thanks to the tumour specific conditions, hence based on the more elevated temperature [7] of tumorous tissues, on their acidity [8], on their reductive character due to the elevated concentration of glutathione [9] or thanks to the presence of tumour-specific enzymes [10]. Such systems are called photo molecular beacons.

Among the different types of photosensitisers, phthalocyanines exhibit particularly sought properties: an intense absorption in the NIR allowing excitation at wavelengths in the phototherapeutic window, easy tailoring of the solubility and easy functionalization for possible coupling to targeting units. A very few phthalocyanines have been designed to be specifically photo-active at the tumour site.

A phthalocyanine substituted by a 2,4-dinitrobenzenesulfonate group, which quenches the electronic events leading to singlet oxygen generation, has been reported [11]. The 2,4-dinitrobenzenesulfonate group is cleaved by glutathione, allowing the photodynamic effect only at the tumour site. With the same principle, phthalocyanine substituted by a ferrocenyl unit via a disulfide linker was reported [12], and, later on, a dual activation strategy was reported [13]. Rather than linking the photosensitiser to a quencher specifically cleaved at the tumour, another possibility is to prepare dimeric systems in which two photosensitisers are connected by a tumour-specific cleavable bond. The linker maintains the two photosensitisers close enough to each other in order to promote a self-quenching of their photoproperties. They are then monomerized at the tumour and their ability to photodynamically generate singlet oxygen is recovered. This has been nicely applied to pheophorbide a-based systems [14].

As we are strongly involved in photosensitising systems based on phthalocyanines [15], this tumour site activation strategy appeared to be an interesting option. It is known indeed that dimeric phthalocyanines are more aggregated than monomeric ones [16–18], inducing a self-quenching of their photoproperties. This prompted us to design dimeric phthalocyanines linked by a disulfide-based linker. Preparing its dimethylene analogue was then necessary to assess the relevance of the concept. As phthalocyanines are, in most of cases, prepared from phthalonitriles derivatives, we designed the bisphthalonitriles **1** and **2** (Scheme 1). Some detailed analyses can be hampered by the limited solubility of phthalocyanines (an issue even worse for dimeric species), and it can then be judicious to analyze the structure of corresponding phthalonitriles [19,20]. A comparative spectroscopic characterization of these two different bisphthalonitriles was hence performed. The crystallographic structure of bisphthalonitrile **1** could be obtained and described in a detailed manner. If suitable crystals of **2** could unfortunately not be obtained, comparative DFT calculations for the structure optimization and electronic structure calculations of **1** and **2** were conducted.

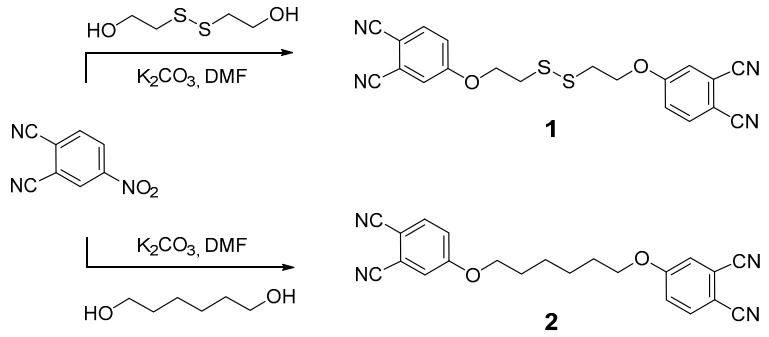

Scheme 1. Synthesis of compound **1** and **2**.

2. Results and Discussion

2.1. Synthesis

Bisphthalonitriles **1** and **2** were both obtained by a double nucleophilic substitution on 4-nitrophthalonitrile, respectively, by 2-hydroxyethyldisulfide and 1,6-hexanediol (Scheme 1). Similar reactions performed by simple alcohols are usually around 60%–70%, and the 42% yield obtained for derivative **2** is, therefore, in accordance with this average, given that a double reaction is achieved. On the contrary, the yield was significantly lower for compound **1**, probably due to a partial degradation of the disulfide bond in the reaction conditions.

2.2. Vibrational and NMR Spectroscopy

FT-IR spectra of both derivatives were recorded (Figure 1). The presence of the S–S function is reflected by the peak at 525 cm^{-1}, which is characteristic but in the fingerprint area of the spectrum. Other parts of the spectra are similar, as can be expected, given that both structures are similar otherwise.

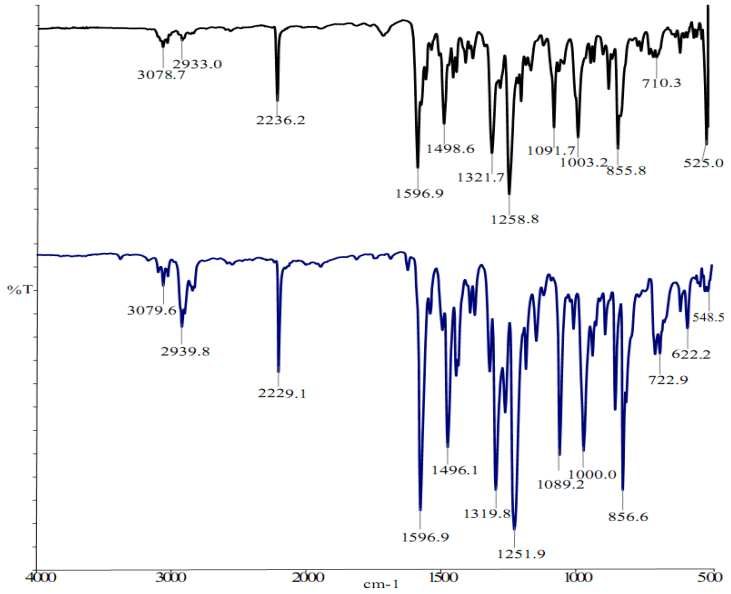

Figure 1. FT-IR spectra of disulfide bridged bisphthalonitrile **1** (**top**, black) compared to reference bisphthalonitrile **2** (**bottom**, blue).

To avoid overlaps of solvent residual peaks with chemical shifts of the investigated bisphthalonitriles, ^{1}H (Figure 2) and ^{13}C (Figure 3) NMR spectra were recorded in deuterated DMSO. The resonance of the aromatic protons is not affected by the presence of the S–S function. A slight shift of the OCH_2 protons' resonance towards low fields can be observed for bisphthalonitrile **1** compared to **2**, the corresponding triplet being centred at 4.40 ppm for **1** and at 4.15 ppm for **2**, due to the electronegativity of the disulfide function. This deshielding effect is even more significant for the OCH_2CH_2 protons, which resonate, respectively, at 3.18 ppm for **1** due to their proximity with the S–S function, and 1.76 ppm for **2**.

Chemical shifts of the aromatic carbons are not significantly affected by the presence of the disulfide function, as one can expect (Figure 2). Resonance of the OCH_2 carbon is shifted by 2 ppm, corresponding to a deshielding effect of the S–S. This effect is even more pronounced for the OCH_2CH_2 as a shift of 8.6 ppm towards low fields can be observed.

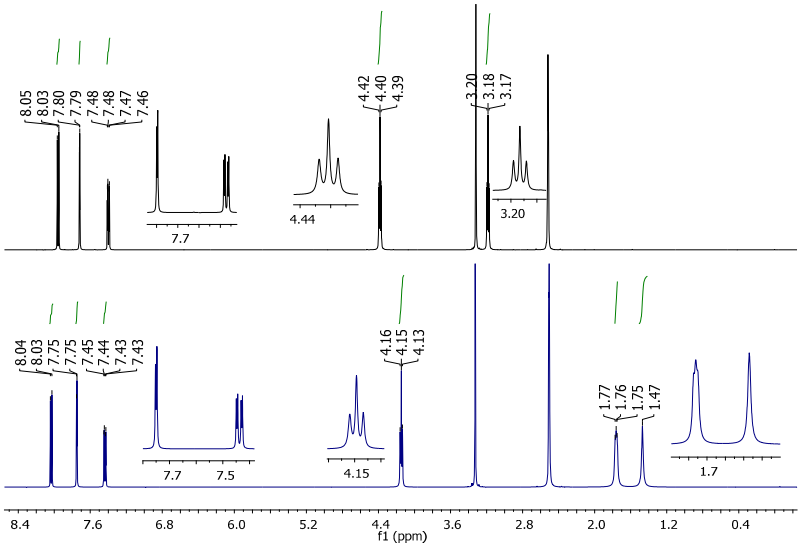

Figure 2. ^{1}H NMR (DMSO-d_6) spectra of disulfide bridged bisphthalonitrile **1** (**top**, black) compared to reference bisphthalonitrile **2** (**bottom**, blue).

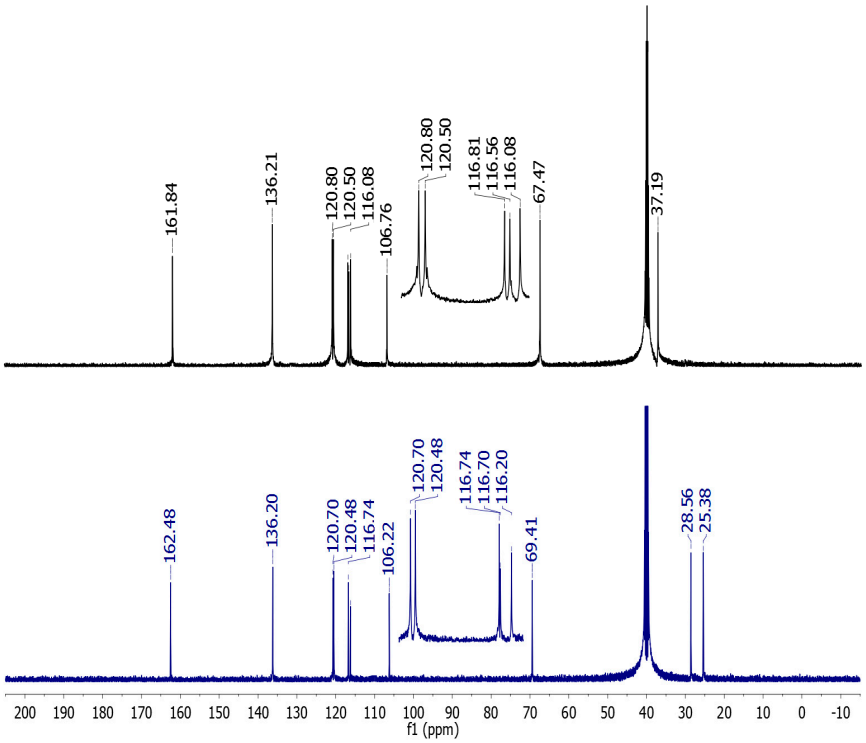

Figure 3. ^{13}C NMR (DMSO-d6) spectra of disulfide bridged bisphthalonitrile **1** (**top**, black) compared to reference bisphthalonitrile **2** (**bottom**, blue).

2.3. Single-Crystal Structural Analysis

The solid-state structure of compound **1** was solved and refined using single-crystal X-ray diffraction data. Suitable crystals of compound **1** have been obtained by slow diffusion of dichloromethane. ORTEP representations of the structure are represented in Figure 4. Compound **1** crystallizes in the triclinic system with P 1 space group. Data collection conditions as well as refinement results are presented in Table 1. The asymmetric unit of the compound includes only one molecule. The intermolecular interactions for bisphthalonitrile **1** are presented in Table 2. Selected bond lengths are tabulated in Table 3 and selected angles are displayed in Table 4.

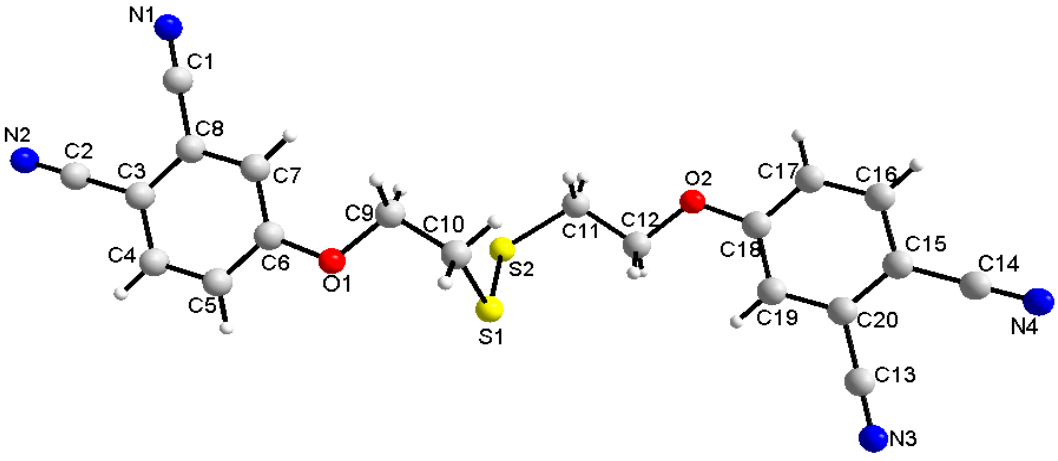

Figure 4. Molecular structure of bisphthalonitrile **1** with 50% probability for ellipsoids.

Table 1. Crystal structure parameters and structural refinement results for bisphthalonitrile **1**.

Empirical Formula	**$C_{20}H_{14}N_4O_2S_2$**
Formula weight	406.4780
Temperature (K)	299
Crystal system	Triclinic
Space group	P 1
a (Å)	5.3047(3)
b (Å)	9.4281(5)
c (Å)	10.3733(6)
β(°)	79.443(4)
Volume ($Å^3$)	488.84(5)
Z	1
λ (Mo Kα)(Å)	0.71073
Crystal shape	Block
Crystal colour	Colourless
Crystal size (mm^3)	0.359 × 0.159 × 0.116
ρ (calc, g/cm^3)	1.381
Absorption coeff. (mm^{-1})	0.296
F(000)	210.0
Reflections collected	7730
Independent reflections	3697
Rint (merging R value)	0.0213
Absorption correction	multi-scan
Data/Restrains/Parameters	3697/3/253
R/Rw (F > 3σF)	0.0353/0.0874
Goodness-of-fit on F	1.031
Δρmin/Δρmax ($e^-.Å^{-3}$)	−0.143/0.265
CCDC number	1061336

Table 2. The intermolecular C–H···N and C–H···O interaction parameters (Å and °) for compound **1**.

D–H···A	**Symmetry**	**d(D–H)**	**d(H···A)**	**d(D–H···A)**	**D–H···A**
C5–H5....O2	−1 + x, 1 + y, z	0.9300	2.6200	3.547(4)	171.800
C7–H7....N3	1 + x, 1 + y, −1 + z	0.9300	2.4900	3.390(5)	163.200
C9–H9B....S2	x, y, z	0.9700	2.9100	3.401(4)	112.700
C17–H17....O1	1 + x, −1 + y, z	0.9300	2.6300	3.553(4)	172.300
C19–H19....N1	−1 + x, −1 + y, 1 + z	0.9300	2.5000	3.398(5)	161.500

Table 3. Selected bond lengths for compound **1** (Å).

C13–N3	1.137(5)
C14–N4	1.138(5)
C6–O1	1.352(4)
O1–C9	1.438(4)
C10–S1	1.812(4)
S1–S2	2.029(3)
S2–C11	1.817(3)
C12–O2	1.433(4)
C18–O2	1.357(4)

Table 4. Selected angles for compound **1**.

C5–C6–C7	119.6(3)
C5–C6–O1	116.3(3)
C6–O1–C9	118.2(3)
C10–S1–S2	103.9(4)
S1–S2–C11	103.4(2)
C12–O2–C18	119.0(2)
C20–C15–C16	118.9(3)
C20–C15–C14	121.4(3)

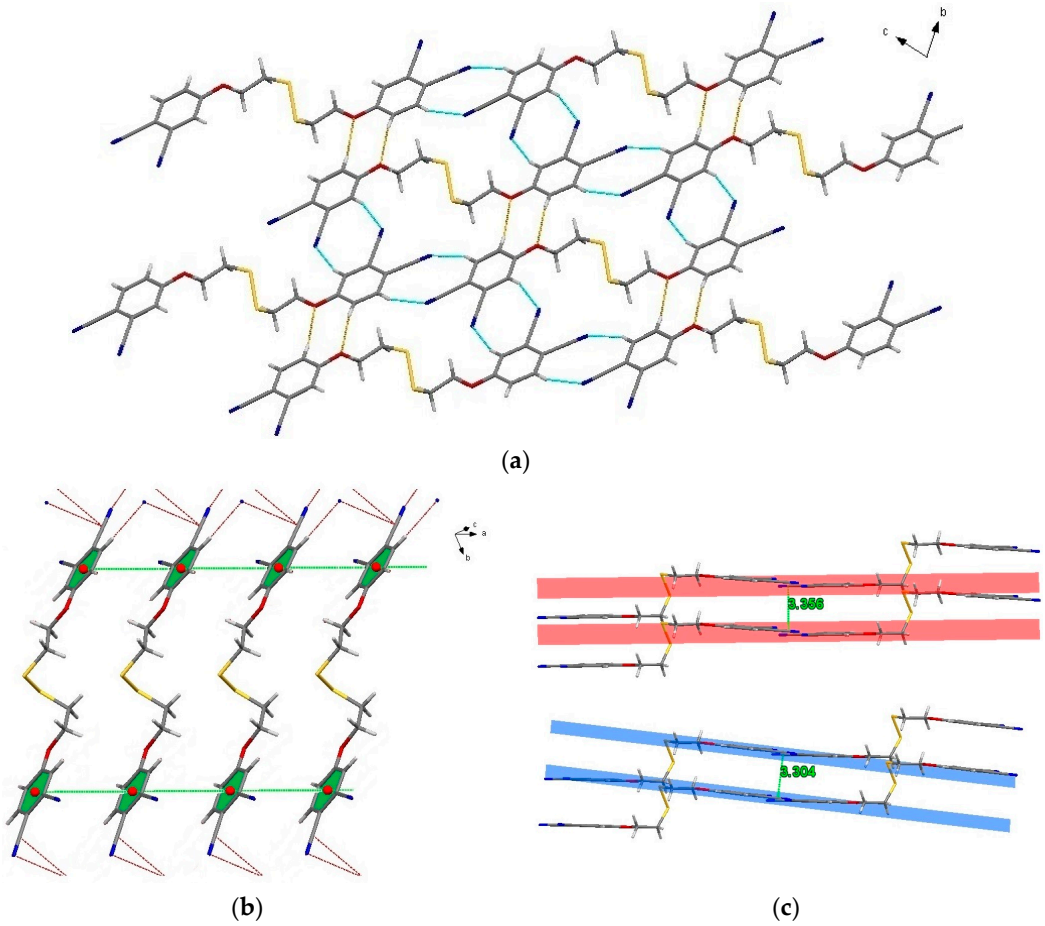

(**a**)

(**b**) (**c**)

Figure 5. Perspective views of (**a**) the C–H···N (**blue** dotted lines), C–H···O (**orange** dotted lines), and (**b**) π···π (**green** dotted lines) and C–N···C (**red** dotted lines) interactions (**c**) interplanar distance (**green** dotted lines) in **1**.

For bisphthalonitrile **1**, in the crystal lattice, C–H···N and C–H···O interactions lead to the formation of two-dimensional sheets in the (*b*,*c*)-plane of the unit-cell. As shown in Figure 5a, infinite molecular chains linked by intermolecular C4–H4···N4, C7–H7···N3 and C16–H16···N2, C19–H19···N1 interactions between cyano groups are connected by C5–H5···O2 and C17–H17···O1 interactions, which leads to a two-dimensional hydrogen bonding network. For the formation of the 3D network, slipped aromatic π···π interactions are essential. Strong attractive interactions between π systems are one of the principal non-covalent forces controlling such varied phenomena, which stabilize the packing of aromatic molecules in crystal. The parallel-displaced configuration is the one of most well-known favourable configurations [21–25]. Slipped aromatic π–π interactions are observed in the crystal structure of **1** as the main stacking interactions that lead to parallel-displaced configurations in the crystals. This predominant behaviour is common for bisphthalonitriles previously reported and

linked by different aliphatic spacers in which only the grafting atom varies (O/S/SO2) [26], but unlike bisphthalonitriles with aromatic spacers (catechol, resorcinol, hydroquinone, phloroglucinol) [21]. From all of these reports, the flexibility of the spacer appears to be more decisive than its length or the nature of the grafting atoms. These interactions are completed by C–N···C interactions, where the distance is 3.237(66) Å (Figure 5b) generating three-dimensional supramolecular network.

The intermolecular stacking of bisphthalonitrile **1** is promoted by the π–π interactions between phthalonitrile aromatic rings, the centroid-centroid distance being (dc-c) 5.305(3) Å between two phthalonitrile aromatic units, a value longer than for related bisphthalonitriles [21–26]. In particular, compared to bisphthalonitriles with spacer having oxygen grafting atom, it appears that this unusually long centroid-centroid distance is more due to the bended geometry of the disulfite function that to the number of atoms in the spacer or to its aliphatic or aromatic character. One can therefore conclude that the disulfide group dramatically influences the crystal packing. The interplanar distances between two phthalonitrile aromatic rings are 3.35 Å (pink colored in Figure 5c) and 3.30 Å (blue colored in Figure 5c). The C≡N bond distances of the bisphthalonitrile range from 1.137(5) to 1.138(6) Å, and these values are in good agreement with those reported in the literature [19–28] except C1–N1 bond distance is 1.129(50) Å shorter than expected. In addition, the data are similar to those observed for unsubstituted phthalonitrile [29], evidencing that the molecular intrinsic structure of the phthalonitrile ring is not affected by the presence of the substituents. C(sp3)–O distances are equal to 1.432(44) Å and 1.438(44) Å, whereas C(sp2)–O distances are slightly shorter than the previous ones, equal to 1.352(36) Å and 1.357(33) Å as expected (Table 2). In bisphthalonitrile **1**, S . . . S distance is 2.029(12) shorter than the sum of the van der Waals radii (3.70 Å). C–S bond lengths and C–O bond lengths of the structure are in good agreement with those reported previously in the literature for comparable molecules [27,30]. C–C–C angles ranging from 118.9(3)° to 121.4(3)° for phenyl ring as expected. The phthalonitrile ring with the conjunction oxygen atom O1 is quite planar (plane equation: −0.6462x − 0.06166y − 0.04496z = −9.8339) and the largest deviation is 0.039 Å. A second phthalonitrile ring with the conjunction oxygen atom O2 is also fairly planar (plane equation: −0.6308x − 0.6681y − 0.3946z = −6.7231) and the largest deviation is 0.039 Å. The value of C6–O1–C9–C10 torsion angle is −178.98(29)°, C18–O2–C12–C11 is 172.46(28)° and C10–S1–S2–C11 is 73.318(18)° are consistent with the value observed in the related phthalonitrile recently reported [31].

2.4. DFT Calculations

In order to estimate the relative stability of the two molecules, we performed structure optimization calculations and determined their total energies in their ground state. The atomization energies of the compounds are calculated, and the reference energies for isolated atoms are obtained from spin polarized calculations. The atomization energy of bisphthalonitrile **2** is found to be 238.017 eV for the whole molecule while that of disulfide bridged bisphthalonitrile **1** is 217.848 eV. Since the numbers of atoms are different, a better criterion is atomization energy per atom. The atomization energy per atom for bisphthalonitrile **2** is 5.17 eV/atom, and for bisphthalonitrile **1** it becomes 5.18 eV/atom. Thus, the two systems are almost equally stable in terms of atomization energies.

The electronic structures and fundamental energy gaps of the bisphthalonitriles **1** and **2** are calculated in order to compare their air-stability. The HOMO-LUMO gap of bisphthalonitrile **2** is found to be 3.29 eV, and that of the disulfide bridged bisphthalonitrile is 3.24 eV in our GGA calculations. These values are close to those of a related derivative with a shorter spacer (three carbon atoms instead of six) previously reported [24]. In our hybrid exchange-correlation functional based calculations, these values are found to be 4.31 eV and 4.27 eV, respectively. Thus, the air-stability of the two molecules should be very similar. The frontier orbitals of the bisphthalonitriles are shown as 3D isosurfaces in Figure 6 for comparison. They both have very similar lowest occupied molecular orbital (LUMO) and LUMO+1 levels, which show π-state character on the carbon rings. These two levels have anti-bonding contribution on the C–N bonds. The highest occupied molecular orbital (HOMO) state for bisphthalonitrile **2**, as shown in Figure 6a, also has π character but with an alternative pattern that has

bonding contribution on the C–N bonds. The HOMO level of the disulfide bridged bisphthalonitrile **2**, as shown in Figure 6b, is quite different, although the energy gaps of the two systems are very similar. In contrast to that of bisphthalonitrile **2**, which had no contribution from the bridging part of the molecule to the HOMO level, it mainly consists of bonding states on the disulfide bridge, and indicates a π-bonding contribution from the S atoms. The HOMO-1 level of the disulfide bridged bisphthalonitrile **2** seems to be a mixture of π-states on the carbon ring and on the disulfide bridge. Therefore, the disulfide bridge should be the active site in bisphthalonitrile **1**.

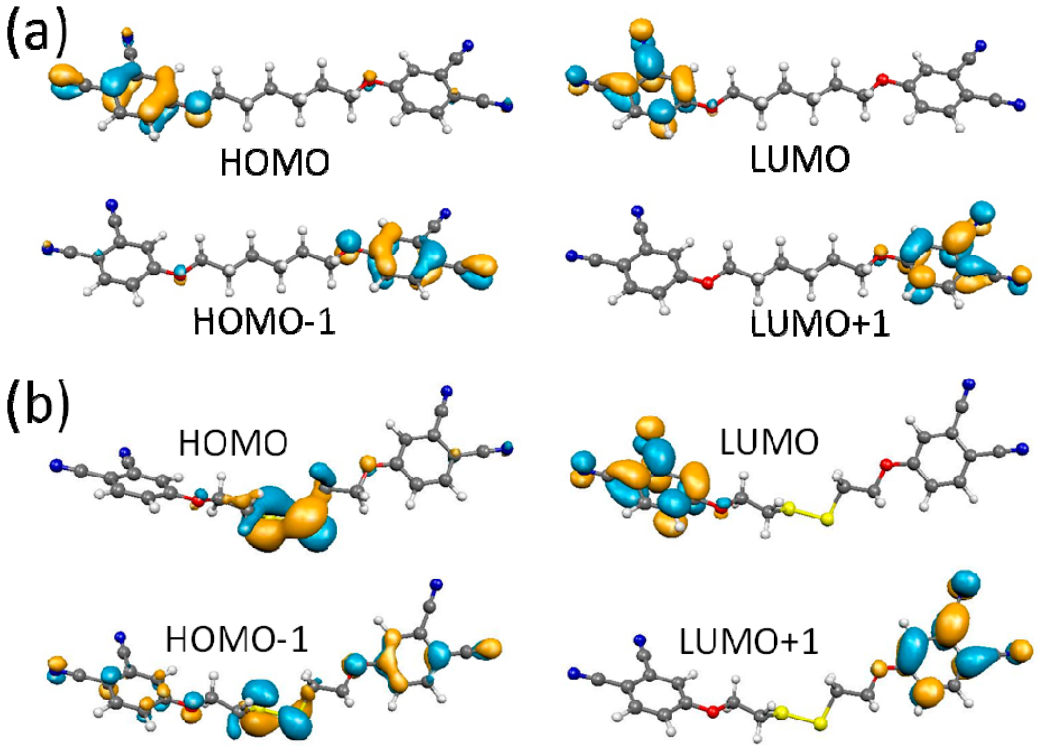

Figure 6. Frontier orbitals for reference bisphthalonitrile **2** (**a**) and for disulfide-linked bisphthalonitrile **1** (**b**) are depicted as 3D isosurfaces.

3. Materials and Methods

3.1. Synthesis

4-Nitrophthalonitrile [32] was synthesized according to published procedure. Solvents and chemicals were purchased from Aldrich (Taufkirchen, Germany) or Alfa Aesar (Karlsruhe, Germany) and used as received. All reaction solvents were dried and purified as described by Perrin and Armarego [33]. Potassium carbonate was dried before used. Melting points were recorded on a Stuart Melting Point smp3 device (Staffordshire, UK). Mass spectra were recorded on a MALDI (matrix assisted laser desorption ionization) BRUKER Microflex LT (Bremen, Germany) using 1,8,9-Anthracenetriol as the matrix. IR spectrum was recorded between 4000 and 500 cm^{-1} using a Perkin-Elmer Spectrum 100 FT-IR spectrometer (PerkinElmer, Italy). ^{1}H NMR and ^{13}C NMR spectra were recorded in DMSO-d_6 solutions on a Varian 500 MHz spectrometer.

Preparation of bisphthalonitrile **1**. 4-nitrophthalonitrile (5.19 g, 0.03 mol, 3 eq.), bis (2-hydroxyethyl) disulfide (1.22 mL, 0.01 mol, 1 eq.) and K_2CO_3 (11 g, 0.08 mol, 8 eq.) were stirred in *N*,*N*-dimethylformamide (20 mL) overnight at room temperature. The reaction mixture was poured into water, the resulting precipitate was filtrated, recovered in dichloromethane, and dried over Na_2SO_4. The product was then purified over silica gel column chromatography (elution gradient,

from hexane to 4 dichloromethane/1 hexane). White solid. Yield: 16% (650 mg). $C_{20}H_{14}N_4O_2S_2$, *M*w 524.65. m.p. 127 °C. FT-IR (cm^{-1}): 3078.7, 3046.3, 2933.0, 2236.2, 1596.9, 1583.4, 1498.6, 1464.3, 1452.7, 1321.7, 1258.8, 1213.1, 1176.4, 1091.7, 1003.2, 955.0, 888.3, 855.8, 767.5, 710.3, 622.2, 525.0. ^{1}H NMR (DMSO-d_6, δ ppm): 8.04 (d, 2H, ^3J = 8.8 Hz), 7.80 (d, 2H, ^3J = 2.5 Hz), 7.47 (dd, 2H, ^3J = 8.8, 2.7 Hz), 4.40 (t, 4H, ^3J = 6.2 Hz), 3.18 (t, 4H, ^3J = 6.2 Hz). ^{13}C NMR (DMSO-d_6, δ ppm): 161.84, 136.21, 120.80, 120.50, 116.81, 116.56, 116.08, 106.76, 67.47, 37.19.

Preparation of bisphthalonitrile **2**. 4-nitrophthalonitrile (20 g, 0.115 mol, 4 eq.) and dry K_2CO_3 (38 g, 0.28 mol, 10 eq.) in *N*,*N*-dimethylformamide (100 mL) was added. After this 1,6-hexanediol (3.3 g, 0.028 mol, 1 eq.) was added to a homogeneous mixture and stirred at room temperature for 72 h. The reaction mixture was poured into water, the resulting precipitate was filtrated and purified by silica gel column chromatography (eluent: 1 dichloromethane/1 hexane), yielding 42% (4.2 g) of a cream-colored solid. $C_{22}H_{18}N_4O_2$, M_W 370.412. m.p. 175 °C. FT-IR cm^{-1}: 3079.6, 3051.2, 2939.8, 2871.6, 2229.1, 1596.9, 1560.7, 1496.1, 1468.1, 1431.0, 1319.8, 1282.9, 1251.9, 1206.0, 1180.8, 1169.3, 1089.2, 1000.0, 897.3, 856.6, 831.0, 746.5, 722.9, 707.4, 650.1, 622.2, 548.9. MS (MALDI-TOF): m/z: 392.27 $[M + Na]^+$, 370.33 $[M]^+$. ^{1}H NMR (DMSO-d_6, δ ppm): 8.03 (d, 2H, ^3J = 8.8 Hz), 7.75 (d, 2H, ^3J = 2.6 Hz), 7.44 (dd, 2H, ^3J = 8.9, 2.6 Hz), 4.15 (t, 4H, ^3J = 6.4 Hz), 1.81–1.70 (m, 4H), 1.47 (s, 4H). ^{13}C NMR (125 MHz, DMSO-d_6, δ ppm): 162.48, 136.20, 120.70, 120.48, 116.74, 116.70, 116.20, 106.22, 69.41, 28.56, 25.38.

3.2. X-Ray Crystallography

Single crystal X-ray diffraction analysis of bisphthalonitrile **1** was carried out on a Bruker APEX II QUAZAR three-circle diffractometer (Madison, WI, USA) using monochromatized Mo Kα X-radiation (λ = 0.71073 Å) using the ϕ and ω technique. Space groups were determined using XPREP (version 2014/2, Bruker, Madison, WI, USA) implemented in APEX2 (version 2014, Bruker, Madison, WI, USA) [34]. All non-hydrogen atoms were refined anisotropically by full-matrix least-squares techniques on F. All other H atoms were generated geometrically and included in the refinement in a riding model approximation. Experimental absorption correction was performed with multi-scan [35]. The crystallographic data are summarized in Table 1. Table 2 represents intermolecular interactions, Table 3 summarizes important bond lengths and selected angles are displayed in Table 4. CCDC-1061336 contains the supplementary crystallographic data for this paper. These data can be obtained free of charge from The Cambridge Crystallographic Data Centre via www.ccdc.cam.ac.uk/data_request/cif.

3.3. Computational

Structure optimization and electronic structure calculations are performed in density functional theory. We use the revised Perdew–Burke–Ernzerhof (revPBE) [36] Generalized Gradient Approximation (GGA) functional for exchange-correlation as implemented in the SIESTA [37] code (version 2.0.2). Electronic wavefunctions are expanded to a double-ζ basis set augmented by polarization orbitals. The interaction between the core and valence electrons are handled by Troullier–Martins norm-conserving pseudopotentials [38] in their fully separable form [39]. Geometry optimizations in the conjugate-gradient algorithm are continued until all force components on each atom are less than 0.01 eV/Å. Since GGA underestimates fundamental energy gaps, electronic energy levels are calculated also in HSE06 hybrid exchange-correlation functional using 6-311G** basis set as implemented in NWChem computer code (version 6.5 , Pacific Northwest National Laboratory, Richland, WA, USA) [40]. Atomization energies are calculated with respect to spin polarized isolated atoms.

4. Conclusions

A disulfide-linked phthalonitrile was designed to serve as a further precursor of specifically tumour-activatable phthalocyanine-based photosensitising systems. Bisphthalonitrile **1** with a disulfide-based linker and its dimethylene analogue **2** were comparatively analyzed on a spectroscopic point of view. FT-IR spectroscopic analysis gave similar observations except for one peak in the

fingerprint area of the spectrum, while NMR analyses showed a marked effect of the disulfide function. DFT calculations indicated also a π-bonding contribution from the S atoms. The thorough crystallographic analysis of disulfide-linked bisphthalonitrile **1** was conducted, allowing an exhaustive characterization of a novel type of bisphthalonitrile.

Supplementary Materials: The following are available online at http://www.mdpi.com/2073-4352/6/8/89/s1, cif and checkcif files for compound **1** (CCDC-1061336).

Acknowledgments: The Scientific and Technological Research Council of Turkey (TUBITAK) is gratefully acknowledged (project 214Z099).

Author Contributions: Fabienne Dumoulin conceived and designed the experiments; Serkan Alpugan, Gülçin Ekineker and Vefa Ahsen performed the syntheses and characterizations; Emel Önal determined the crystal structure; Savaş Berber performed the calculations; all authors contributed to the paper's writing.

Conflicts of Interest: The authors declare no conflict of interest.

References

1. Triesscheijn, M.; Baas, P.; Schellens, J.H.M.; Stewart, F.A. Photodynamic therapy in oncology. *Oncologist* **2006**, *11*, 1034–1044. [CrossRef] [PubMed]
2. Chen, X.Q.; Song, H.T.; Chen, S.P.; Zhang, J.; Niu, G.X.; Liu, X.N. Clinical efficacy of 5-aminolevulinic acid photodynamic therapy in the treatment of moderate to severe facial acne vulgaris. *Exp. Ther. Med.* **2015**, *10*, 1194–1198. [CrossRef] [PubMed]
3. Ideta, R.; Tasaka, F.; Jang, W.D.; Nishiyama, N.; Zhang, G.D.; Harada, A.; Yanagi, Y.; Tamaki, Y.; Aida, T.; Kataoka, K. Nanotechnology-Based Photodynamic Therapy for Neovascular Disease Using a Supramolecular Nanocarrier Loaded with a Dendritic Photosensitizer. *Nano Lett.* **2005**, *5*, 2426–2431. [CrossRef] [PubMed]
4. Maisch, T. Strategies to optimize photosensitizers for photodynamic inactivation of bacteria. *J. Photochem. Photobiol. B Biol.* **2015**, *150*, 2–10.
5. Jiang, Z.; Shao, J.W.; Yang, T.T.; Wang, J.; Jia, L. Pharmaceutical development, composition and quantitative analysis of phthalocyanine as the photosensitizer for cancer photodynamic therapy. *J. Pharm. Biomed. Anal.* **2014**, *87*, 98–104. [CrossRef] [PubMed]
6. Maruani, A.; Savoie, H.; Bryden, F.; Caddick, S.; Boyle, R.; Chudasama, V. Site-selective multi-porphyrin attachment enables the formation of a next-generation antibody-based photodynamic therapeutic. *Chem. Commun.* **2015**, *51*, 15304–15307. [CrossRef] [PubMed]
7. Chen, Z.; Xu, P.; Chen, J.; Chen, H.; Hu, P.; Chen, X.; Lin, L.; Huang, Y.; Zheng, K.; Zhou, S.; et al. Zinc phthalocyanine conjugated with the amino-terminal fragment of urokinase for tumor-targeting photodynamic therapy. *Acta Biomater.* **2014**, *10*, 4257–4268. [CrossRef] [PubMed]
8. Walker, M.D.; Thomas, D.G.T. *Biology of Brain Tumour*; Martinus Nijhof: Leiden, The Netherlands; Boston, MA, USA, 1986.
9. Jiang, X.J.; Lo, P.C.; Tsang, Y.M.; Yeung, S.L.; Fong, W.P.; Ng, D.K.P. Phthalocyanine-Polyamine Conjugates as pH-Controlled Photosensitizers for Photodynamic Therapy. *Chem. Eur. J.* **2010**, *16*, 4777–4783. [CrossRef] [PubMed]
10. Isık, M.; Guliyev, R.; Kolemen, S.; Altay, Y.; Senturk, B.; Tekinay, T.; Akkaya, E.U. Designing an Intracellular Fluorescent Probe for Glutathione: Two Modulation Sites for Selective Signal Transduction. *Org. Lett.* **2014**, *16*, 3260–3263. [CrossRef] [PubMed]
11. Gabriel, D.; Lange, N.; Chobaz-Peclat, V.; Zuluaga, M.F.; Gurny, R.; van den Bergh, H.; Busso, N. Thrombin-sensitive dual fluorescence imaging and therapeutic agent for detection and treatment of synovial inflammation in murine rheumatoid arthritis. *J. Control. Release* **2012**, *163*, 178–186. [CrossRef] [PubMed]
12. He, H.; Lo, P.-C.; Ng, D.K.P.A. Glutathione-Activated Phthalocyanine-Based Photosensitizer for Photodynamic Therapy. *Chem. Eur. J.* **2014**, *20*, 6241–6245. [CrossRef] [PubMed]
13. Lau, J.T.F.; Jiang, X.-J.; Ng, D.K.P.; Lo, P.-C. A disulfide-linked conjugate of ferrocenyl chalcone and silicon (IV) phthalocyanine as an activatable photosensitiser. *Chem. Commun.* **2013**, *49*, 4274–4276. [CrossRef] [PubMed]
14. Lau, J.T.F.; Lo, P.-C.; Jiang, X.-J.; Wang, Q.; Ng, D.K.P. A Dual Activatable Photosensitizer toward Targeted Photodynamic Therapy. *J. Med. Chem.* **2014**, *57*, 4088–4097. [CrossRef] [PubMed]

15. Kim, W.L.; Cho, H.; Li, L.; Kang, H.C.; Huh, K.M. Biarmed Poly (ethylene glycol)-(pheophorbide a)2 Conjugate as a Bioactivatable Delivery Carrier for Photodynamic Therapy. *Biomacromolecules* **2014**, *15*, 2224–2234. [CrossRef] [PubMed]
16. Tuncel, S.; Trivella, A.; Atilla, D.; Bennis, K.; Savoie, H.; Albrieux, F.; Delort, L.; Billard, H.; Dubois, V.; Ahsen, V.; et al. Assessing the Dual Activity of a Chalcone—Phthalocyanine Conjugate: Design, Synthesis, and Antivascular and Photodynamic Properties. *Mol. Pharm.* **2013**, *10*, 3706–3716. [CrossRef] [PubMed]
17. Işci, Ü.; Beyreis, M.; Tortik, N.; Topal, S.Z.; MGlueck, M.; Ahsen, V.; Dumoulin, F.; Kiesslich, T.; Plaetzer, K. Methylsulfonyl Zn phthalocyanine: A polyvalent and powerfulhydrophobic photosensitizer with a wide spectrum of photodynamicapplications. *Photodiagn. Photodyn. Ther.* **2016**, *13*, 40–47. [CrossRef] [PubMed]
18. Lafont, D.; Zorlu, Y.; Savoie, H.; Albrieux, F.; Ahsen, V.; Boyle, R.W.; Dumoulin, F. Monoglycoconjugated Phthalocyanines. Effect of Sugar and Linkage on Photodynamic Activity. *Photodiagn. Photodyn. Ther.* **2013**, *10*, 252–259. [CrossRef] [PubMed]
19. Yu Tolbin, A.; Tomilova, L.G.; Zefirov, N.S. Bi- and polynuclear phthalocyanines: Synthesis and study of physicochemical properties. *Russ. Chem. Rev.* **2008**, *77*, 435–449. [CrossRef]
20. Makhseed, S.; Machacek, M.; Alfadly, W.; Tuhl, A.; Vinodh, M.; Simunek, T.; Novakova, V.; Kubat, P.; Rudolf, E.; Zimcik, P. Water-soluble non-aggregating zinc phthalocyanine and in vitro studies for photodynamic therapy. *Chem. Commun.* **2013**, *49*, 11149–11151. [CrossRef] [PubMed]
21. Köç, M.; Zorlu, Y.; İşci, Ü.; Berber, S.; Ahsen, V.; Dumoulin, F. A library of dimeric and trimeric phthalonitriles linked by a single aromatic ring: Comparative structural and DFT investigation. *CrystEngComm* **2016**, *18*, 1416–1426. [CrossRef]
22. Sinnokrot, M.O.; Valeev, E.F.; Sherrill, C.D. Estimates of the Ab Initio Limit for $\pi-\pi$ Interactions: The Benzene Dimer. *J. Am. Chem. Soc.* **2002**, *124*, 10887–10893. [CrossRef] [PubMed]
23. Desiraju, G.R.; Gavezzotti, A. From molecular to crystal structure; polynuclear aromatic hydrocarbons. *J. Chem. Soc. Chem. Comm.* **1989**, 621–623. [CrossRef]
24. Castineiras, A.; Sicilia-Zafra, A.G.; Gonzalez-Perez, J.M.; Choquesillo-Lazarte, D.; Niclos-Gutierrez, J. Intramolecular "Aryl-Metal Chelate Ring" π,π-Interactions as Structural Evidence for Metalloaromaticity in (Aromatic α,α'-Diimine)-Copper(II) Chelates: Molecular and Crystal Structure of Aqua(1,10-phenanthroline) (2-benzylmalonato)copper(II) Three-hydrate. *J. Inorg. Chem.* **2002**, *41*, 6956–6958. [CrossRef]
25. Tsuzuki, S.; Uchimaru, T.; Sugawara, K.; Mikami, M. Energy profile of the interconversion path between T-shape and slipped-parallel benzene dimers. *J. Chem. Phys.* **2002**, *117*, 11216–11221. [CrossRef]
26. Ekineker, G.; Pilet, G.; Berber, S.; Ahsen, V.; Dumoulin, F.; Önal, E. Spectroscopic and structural properties of bisphthalonitriles with O/S/SO2 grafting: Comparative theoretical and experimental studies. *J. Mol. Struct.* **2016**, *1123*, 261–270. [CrossRef]
27. Zorlu, Y.; Taşkıran, D.T.; Tarakçı, D.K.; Kumru, U.; Alpugan, S.; İşçi, Ü.; Dumoulin, F.; Ahsen, V. Dihydroxylated Alkylsulfanyl Phthalonitriles. *J. Chem. Crystallogr.* **2014**, *44*, 337–345. [CrossRef]
28. Zeng, W.-L.; Xin, C.-H. Synthesis and Crystal Structure of 4-(2-Isopropyl-5-methylcyclohexyloxy) phthalonitrile. *Asian J. Chem.* **2013**, *25*, 2067–2069.
29. Janczak, J.; Kubiak, R. 1,2-Dicyanobenzene. A Precursor of Phthalocyanines. *Acta Crystallogr. Sect. C Cryst. Struct. Commun.* **1995**, *51*, 1399–1401. [CrossRef]
30. Zorlu, Y.; İşci, Ü.; Hirel, C.; Dumoulin, F.; Ahsen, V. Phthalonitriles Functionalized for Click Chemistry. Design, Synthesis and Structural Characterization. *J. Chem. Crystallogr.* **2013**, *43*, 636–645. [CrossRef]
31. Chi, Y.J.; Tan, A.L.; Wimmer, F.L.; Mirza, A.H.; Young, D.J.; Ng, S.W.; Tiekink, E.R.T. 4-(Prop-2-yn-1-yloxy) benzene-1,2-dicarbonitrile. *Acta Cryst. Sec. E* **2012**, *68*, o2293–o2294.
32. Young, J.G.; Onyebuagu, W. Synthesis and characterization of di-disubstituted phthalocyanines. *J. Org. Chem.* **1990**, *55*, 2155–2159. [CrossRef]
33. Perrin, D.D.; Armarego, W.L.F. *Purification of Laboratory Chemicals*, 2nd ed.; Pergamon Press: Oxford, UK, 1989.
34. Bruker. *APEX2*; Bruker AXS Inc.: Madison, WI, USA, 2008.
35. Bruker. *Multi-Scan SADABS (V2014/5)*; Bruker AXS Inc.: Madison, WI, USA, 2014.
36. Perdew, J.P.; Burke, K.; Ernzerhof, M. Generalized Gradient Approximation Made Simple. *Phys. Rev. Lett.* **1996**, *77*, 3865–3868. [CrossRef] [PubMed]
37. Soler, J.M.; Artacho, E.; Gale, J.D.; García, A.; Junquera, J.; Ordejón, P.; Sánchez-Portal, D. The SIESTA method for ab initio order-N materials simulation. *J. Phys. Condens. Matter* **2002**, *14*, 2745–2779. [CrossRef]

38. Troullier, N.; Martins, J.L. Efficient pseudopotentials for plane-wave calculations. *Phys. Rev. B* **1991**, *43*, 1993–2006. [CrossRef]
39. Kleinman, L.; Bylander, D.M. Efficacious Form for Model Pseudopotentials. *Phys. Rev. Lett.* **1982**, *48*, 1425–1428. [CrossRef]
40. Valiev, M.; Bylaska, E.J.; Govind, N.; Kowalski, K.; Straatsma, T.P.; van Dam, H.J.J.; Wang, D.; Nieplocha, J.; Apra, E.; Windus, T.L.; et al. NWChem: A comprehensive and scalable open-source solution for large scale molecular simulations. *Comput. Phys. Commun.* **2010**, *181*, 1477–1489. [CrossRef]